H_2-reduced phosphomolybdate promotes room-temperature aerobic oxidation of methane to methanol

Sikai Wang
National University of Singapore
Victor Fund
Georgia Institute of Technology
Max Hülsey
National University of Singapore https://orcid.org/0000-0002-9894-0492
Xiaocong Liang
Fuzhou University
Zhiyang Yu
Fuzhou University https://orcid.org/0000-0002-8742-752X
Jinquan Chang
National University of Singapore
Andrea Folli
Cardiff University
Richard Lewis
Cardiff University https://orcid.org/0000-0001-9990-7064
Graham Hutchings
Cardiff University
Qian He
National University of Singapore https://orcid.org/0000-0003-4891-3581
Ning Yan (ning.yan@nus.edu.sg)
National University of Singapore https://orcid.org/0000-0002-1877-9206

Article

Keywords:

Posted Date: January 11th, 2023

DOI: https://doi.org/10.21203/rs.3.rs-2307433/v1

Version of Record: A version of this preprint was published at Nature Catalysis on August 31st, 2023. See the published version at https://doi.org/10.1038/s41929-023-01011-5.

Abstract

The selective partial oxidation of methane to methanol using molecular oxygen represents a long-standing challenge in the field of catalysis, inspiring extensive study for many decades However, to date considerable challenges still prevent large-scale production via the aerobic route. Herein, we report a Pd-containing phosphomolybdate catalyst (Pd/CsPMA), which, after activation by H_2 converts methane and O_2 almost exclusively to methanol at room temperature. The highest activity reached 67.4 $\mu molg_{cat}^{-1}h^{-1}$. Pd enables rapid H_2 activation and H spillover to phosphomolybdate for Mo reduction, while facile O_2 and subsequent methane activation occurs on the reduced phosphomolybdate sites. Phosphomolybdate maintained its Keggin-type structure during the reaction, and the catalyst is reused 4 times without losing activity. The work reveals the underexplored potential of Mo-based catalyst for aerobic methane oxidation and highlights the importance of regulating the chemical valance state to construct methane active sites.

Introduction

The selective oxidation of methane to organooxygen chemicals such as methanol using molecular oxygen represents a long-standing challenge in chemistry.[1–4] However, despite decades of research, there is still no industrially viable direct route to methanol production from methane.[5,6] Indeed the large scale methanol production is reliant on the multi-step (syngas) route, which operates at elevated temperatures and pressures.[7] In nature the methane monooxygenase (MMO) class of enzymes represents a one-step aerobic route to methanol that operates under ambient conditions.[8] Many heterogeneous catalysts have also been developed for methane valorization using molecular oxygen as the terminal oxidant,[9–25] with relatively high temperatures typically applied (100–240°C). Considerable attention has been placed on precious metal-based catalysts, for instance, atomically dispersed Rh species has been shown to offer high efficacy when utilizing CO as a co-reductant.[2] By comparison recent investigations have demonstrated the efficacy of supported Au nanoparticles in the absence of a co-reductant.[10] However, in both cases considerable concentrations of further oxidation products (such as acetic and formic acid) are also synthesized.

Alternative approaches to methane oxidation, which operate at mild temperatures, have been investigated. Significant focus in particular has been placed on the utilization of H_2O_2 as the oxidant, which produces hydroxyl (·OH) and hydroperoxyl (·OOH) radicals[21,26,27], or interacts with surface metal sites to generate active oxygen-containing groups to achieve methane activation, with these latter materials able to compete with MMO on an activity basis.[9,17] However, while methane valorization using commercially synthesized H_2O_2 may be promising on an academic scale, the economic and technical challenges associated with H_2O_2 formation via current industrial routes and concerns associated with the safe transport and storage of the oxidant are likely to preclude the utilization of H_2O_2 for methane upgrading on an industrial level.[28] Towards this end, significant recent progress has been made by Jin et al. and others who demonstrated the efficacy of H_2O_2 generated in-situ for methanol synthesis.[21,24,29–31]

Under light irradiation, *in situ* formed ·OH radicals over photocatalysts also initiate effective methane conversion to methanol.[32–34]

To conceive fresh ideas for designing thermal catalysts for methane oxidation, we draw new inspiration from the MMO class of enzymes. During the enzymatic process, a reductase or other electron-donating co-factor partially reduces the Fe or Cu active sites with the MMO, which subsequently interact with O_2 to create active O-containing species for selective methane oxidation.[4,35] We postulate that regulating the chemical valence state of metal sites, in particular to generate partially reduced metal centers, might be a promising strategy which allows for the oxidation potential of O_2 to be harnessed at ambient conditions.

Polyoxometalates (POM), such as phosphomolybdate ($[PMo_{12}O_{40}]^{3-}$, PMA), are a group of inorganic polyatomic ion clusters with numerous catalytic applications.[36–39] Keggin structured PMA is composed of a globelike cluster of a phosphate caged by 12 inter-linked Mo-oxygen clusters with Mo in high oxidation state. By immobilizing Pd onto Mo-based POMs, we previously observed facile reduction of Mo by H spillover from Pd at ambient temperature.[40] Within this study we demonstrate that the caesium-exchanged phosphomolybdate catalyst with Pd immobilized (Pd/CsPMA) offers considerable activity for ambient temperature aerobic oxidation of methane to methanol. Although the as-prepared Pd/CsPMA is inactive, after pre-treatment in H_2 the reduced catalyst (Pd/CsPMA-H) converts methane and O_2 to methanol with ~ 100% selectivity and a productivity of 67.4 $\mu molg_{cat}^{-1}h^{-1}$ activity. The catalyst also produces methanol from methane in a mixed H_2/methane/O_2 atmosphere. In sharp contrast to previous studies where H_2O_2,·OH radicals and/or Pd sites are actively involved in C – H activation of methane,[22,29] our mechanistic studies strongly suggest that activation of O_2 and CH_4 for methanol occurs directly on reduced PMA.

Results And Discussion

Pd/CsPMA: structural features and H_2-reduction/re-oxidation properties.

Pd/CsPMA was prepared by precipitating PMA anions ($[PMo_{12}O_{40}]^{3-}$) with Cs^+ and Pd^{2+} at sub-ambient temperatures. The separated yellow solids, as observed by scanning electronic microscopy (SEM) and transmission electronic microscopy (TEM), are sphere particles with a size approximately ranging from 50 to 300 nm (**Figures S1 and S2**). X-ray diffraction (XRD) results suggest that the Pd/CsPMA material has a cubic crystal structure distinct from those of MoO_3 and PMA (Fig. 1a). From integrated differential phase contrast imaging (iDPC), the crystals are assembled from individual PMA units (Fig. 1b, S3-S5), based on which a structural model of Pd/CsPMA material was constructed (**Figure S6**). Pd/CsPMA and PMA gave similar Raman spectra, suggesting the preservation of the anion structure during catalyst synthesis (Fig. 1c). The actual Pd loading of Pd/CsPMA was determined to be 0.23 wt.% by inductively coupled plasma optical emission spectroscopy. Pd species distribute evenly on Pd/CsPMA, as shown in the high-angle annular dark-field (HAADF) imaging results under STEM mode (Fig. 1d). The X-ray photoelectron spectroscopy (XPS) analysis (Fig. 1e) and *in situ* diffuse reflectance infrared spectroscopy

(DRIFTS) with NO as the probe molecule (Fig. 1f) confirm that Pd exists as charged Pd cations, likely situated at the 4-fold hollow sites of PMA by replacing Cs^+, as indicated in previous studies on single-atom POM systems.[38,41]

When Pd/CsPMA was exposed to forming gas (5% H_2/N_2) flow at room temperature (24 ℃), a rapid color change from yellow to dark blue was observed within twenty minutes. *In situ* H_2-DRIFT spectrum of Pd/CsPMA present a notable peak at above 3200 cm^{-1} for Pd/CsPMA (**Figure S7**), indicating the formation of large amount of surface hydroxyl groups, which is not the case for CsPMA. This implies that Pd plays a crucial role in dissociating H_2 into H atoms and transferring H species from the noble metal sites to the support.[42,43] The H atoms donate electrons to PMA and combine with PMA oxygen to form –OH groups on the surface. *In situ* NO-DRIFTS analysis confirms that Pd species remain highly dispersed during H_2 treatment at room temperature (**Figure S8**). We then prepared a Pd/CsPMA-H material, by treating the Pd/CsPMA under H_2 (4 bar) in water for 15 min. As shown in Fig. 1g, the color of the catalyst also changed from yellow (Pd/CsPMA) to dark blue (Pd/CsPMA-H). UV-Visible (UV-Vis) adsorption spectra of the Pd/CsPMA-H suspension show an obvious decrease of Mo(VI) signal at 320–340 nm and an increase of Mo(V) and Mo(IV) in the range of 600–900 nm, illustrating the reduction of Mo by hydrogen spillover (Fig. 1h).[44,45] Determined by redox titration using acidified $FeCl_3$ solution (**Figure S9**), each POM anion on average accepts 7.5 electrons after 15-minute H_2 treatment, corroborating the UV-Vis adsorption data that Mo(VI) was only partially reduced. Additional H_2 treatment does not increase the degree of hydrogen spillover.

The reduced Pd/CsPMA-H powder readily re-oxidizes when exposed to air at room temperature (represented as Pd/CsPMA-H-O), as judged from the recovered yellowish color and the UV-Vis absorption results (Fig. 1g and 1h). This highlights that the reduced Pd/CsPMA can activate O_2 at ambient temperature. Pd/CsPMA-H-O exhibits similar morphology, crystalline structure, and POM anion characteristic Raman peaks to those of the pristine Pd/CsPMA (**Figure S1, S10, 1a and 1c**), which prove that the repeated reduction-oxidation steps would not change the structure of Pd/CsPMA, thus hinting at its potential as a catalyst in redox reactions.

Catalytic performance in partial methane oxidation. The methane oxidation reaction was carried out at room temperature in an aqueous solution with CH_4 and O_2.[46] The unactivated Pd/CsPMA catalyst exhibited negligible methane conversion activity (Table 1, **Entry 1**), and after reaction the Mo species in Pd/CsPMA maintained an oxidation state of + 6 (**Figure S11**). To validate adding electrons to the catalyst is conducive to aerobic oxidation of methane, Pd/CsPMA was first treated by H_2 in the liquid phase at room temperature to form the reduced catalyst, Pd/CsPMA-H. When Pd/CsPMA-H was used for methane oxidation with O_2 under identical conditions for 30 mins, we observed methane conversion with methanol as the sole product (5.2 $\mu mol g_{cat}^{-1} h^{-1}$) (Table 1, **Entry 2**). Shorting the reaction to 5 minutes provided proportionally increased methanol production rate (28.8 $\mu mol g_{cat}^{-1} h^{-1}$), suggesting that Pd/CsPMA-H is only active in the initial stage of reaction (Table 1, **Entry 3**). By adjusting the partial pressure of CH_4 and

O_2, it was possible to improve methanol productivity, with this metric rising to 67.4 $\mu molg_{cat}^{-1}h^{-1}$ (Table 1, **Entry 4**). The color of the spent catalyst changed to greenish yellow, suggesting that they were re-oxidized by O_2 during the course of the reaction (**Figure S11**). These results highlight two important findings. First, H_2-reduced Pd/CsPMA selectively transform methane and O_2 into methanol at room temperature. Second, Pd/CsPMA-H does not maintain its reduced state under an oxidizing atmosphere, thus quickly losing its initial activity.

To sustain a reduced catalyst state, we then attempted the methane oxidation reaction using a non-explosive gas mixture of H_2, O_2, CH_4 and N_2, while H_2 pretreatment was no longer applied. Under an optimized H_2/O_2 ratio, Pd/CsPMA presents a methanol productivity of 28.5 $\mu molg_{cat}^{-1}h^{-1}$ (a noble metal specific productivity of 12.4 $mmolg_{Pd}^{-1}h^{-1}$), again with methanol as the only liquid product detected together with negligible gas-phase product in a 30-minute reaction (Table 1, **Entry 5**). The activity and selectivity are exceptional among most reported noble-metal-containing catalysts for thermal catalytic aerobic oxidation of methane to methanol at room temperature (**Table S1**). Interestingly, we observed that in a typical 30-mins reaction, the reaction proceeds at higher rates in the 2nd 15 mins compared to the 1st, likely due to an induction period required to form the reduced catalyst that is active for methane oxidation (**Figure S12**). The ratio of H_2 and CH_4 almost remained constant during the reaction, suggesting that H_2 is not preferentially consumed by O_2 as compared to CH_4 (**Table S2**).

Table 1

Oxidation of methane to methanol using Pd/CsPMA catalyst. Reaction condition: 2 mL D_2O, 10 mg catalyst, room temperature, 800 rpm. For Entry 1, 10 bar CH_4, 1 bar O_2 and 9 bar N_2 were applied. For Entry 2, 3, 7 and 8, the catalyst was treated with 4 bar of H_2 for 15 min at room temperature before running the reaction under the same condition. For Entry 4, 20 bar of CH_4 was used. For Entry 5, 10 bar CH_4, 4 bar H_2 and 0.3 bar O_2 balanced with 25.7 bar N_2 were applied. For Entry 6, the solvent used was H_2O instead of D_2O. For Entry 7 and 8, 1 µmol of ascorbic acid and Na_2S were added, respectively, after H_2 pretreatment but before charging methane and O_2.

Entry	Condition (number in parenthesis refer to gas pressure. unit: bar)	CH_3OH prod. (µmol g_{cat}^{-1} h^{-1})	CH_3OH Sel.	Specific activity (mmol g_{Pd}^{-1} h^{-1})	Color after reaction
1	Single step: CH_4(10) + O_2(1), 30 min	0	N/A	0	Yellow
2	Step 1: H_2(4); Step 2: CH_4(10) + O_2(1), 30 min	5.2	100.0%	2.3	Yellow
3	Step 1: H_2(4); Step 2: CH_4(10) + O_2(1), 5 min	28.8	100.0%	12.5	Green
4	Step 1: H_2(4); Step 2: CH_4(20) + O_2(0.3) 5 min	67.4	100.0%	29.3	Green
5	Single step: CH_4(10) + H_2(4) + O_2(0.3), 30 min	28.5	100.0%	12.4	Dark blue
6	Single step: CH_4 + H_2O_2(400µmol), 30 min	0	N/A	0	Yellow
7	Single step: H_2(4); Ascorbic acid, CH_4(10) + O_2 (1), 5 min	42.2	100.0%	18.4	Green
8	Single step: H_2(4); Na_2S, CH_4(10) + O_2(1), 5 min	48.0	100.0%	20.9	Blue

Xiao and colleagues previously reported[29] selective methane oxidation with H_2 and O_2 using AuPd particles confined in a zeolite support. In that case, H_2O_2 was produced locally, which then acts as the oxidant for methane oxidation. In contrast, H_2O_2 is unlikely to be the key oxidant in our system, because (i) no H_2O_2 was detected when supplying a mixture of H_2 and O_2 over the catalyst (detection limit: 0.5 ppm, **Figure S13**) and (ii) when external H_2O_2 was added, no methanol was detected after 30 mins despite 54% of the H_2O_2 was decomposed (Table 1, **Entry 6** and **Table S3)**. Methanol was produced only when H_2O_2 was used together with H_2 (**Table S3**), but the best activity (*e.g.*, 14.4 µmol$g_{cat}^{-1}h^{-1}$) was still not as high as the case when H_2 and O_2 are supplied. Molecular O_2 works as a better oxidant than H_2O_2

in our case, possibly because as a weaker oxidant, O_2 allows the catalyst to maintain the desired reduced state under H_2.

Methane oxidation was performed under varied partial pressure of CH_4, H_2, and O_2. The reaction is first order with respect to CH_4 between 0–15 bar (Fig. 2a), indicating methane activation participates in the rate-determining step. On the other hand, the methanol yield as a function of the H_2 to O_2 ratio follows a volcano-type curve, with the optimal pressure of H_2 at 4 bar (Fig. 2b). A threshold of 2 bar H_2 partial pressure must be reached to create a state with sufficient degree of Mo reduction for C – H bond activation. When O_2 is eliminated from the reaction system, methanol was only detected in trace amount (2 $\mu molg_{cat}^{-1}h^{-1}$), likely due to residual O_2 in water.

Several control catalyst samples were studied to confirm the critical role of reduced Mo species as catalyst active sites. CsPMA, Rh/CsPMA and Pt/CsPMA, showing no reduction of PMA by H_2 at room temperature, exhibited no methanol productivity (Fig. 2c). Rh/CsPMA and Pt/CsPMA were then pretreated with H_2 at elevated temperature (50 °C and 100 °C, respectively). After the pretreatment, both catalysts turned dark blue signaling Mo reduction, and in the following step both catalysts produced methanol from methane and oxygen at room temperature (**Table S4**). Replacing PMA by phosphotungstate (PTA), Pd/CsPTA also did not show methane activation under the same conditions (**Figure S7**). To explore whether our finding, i.e., H_2-reduced Mo in Pd/CsPMA readily converts methane and O_2 to methanol, is generalizable, 1 wt.% Pd/MoO_3, 1 wt.% Pd/WO_3 and 10 wt.% Pd/C were evaluated under our methane oxidation conditions (Fig. 2d, **Table S5**). The H_2-pretreated 1 wt.% Pd/MoO_3-H indeed exhibited a methanol productivity of 14.4 $\mu molg_{cat}^{-1}h^{-1}$ in a 5-min reaction, while the other two catalysts were inactive. Interestingly, MoO_2, with Mo(IV) as the only Mo species, showed no methane activation properties with O_2. The above results indicate that Pd is not indispensable for methane activation, but Mo-species under a partially reduced chemical state is a critical element for methane activation with oxygen.

Methanol formation pathway on reduced PMA: experimental evidence. Since radical mechanism is one of the mainstream mechanisms to activate methane C – H bond in aqueous solution, EPR experiments using 5,5-dimethyl-1-pyrroline N-oxide (DMPO) radical trapping agent were performed to determine the presence of reactive oxygen species (**Figure S14**).[47] The appearance of characteristic quadruple peaks (1:2:2:1) for H_2O_2 aqueous solution indicates trapped ·OH radicals, while a triple peak was observed for the aqueous suspension of pristine Pd/CsPMA, probably coming from the oxidative dimerization of DMPO.[48] However, these are the cases where no methanol productivity was observed. By contrast, for the H_2 pretreated Pd/CsPMA-H catalyst, no similar signals were detected. To provide further evidence that ·OH radicals do not operate in our system, methane oxidation reactions were carried out over the Pd/CsPMA-H catalyst in the presence of ·OH radical scavengers (Na_2S or ascorbic acid) (Table 1, **Entry 6–7**). In these cases, the methanol productivity of the Pd/CsPMA-H catalyst did not decrease, but rather increased to 42.2 and 48.0 $\mu molg_{cat}^{-1}h^{-1}$, respectively, compared to the 28.8 $\mu molg_{cat}^{-1}h^{-1}$ without the scavengers. This suggests

that methane is not activated by free ·OH intermediates. The increased productivity may be ascribed to the elongated lifetime for reduced PMA species under O_2, due to the reductivity of scavengers.

To further rule out the role of Pd in C – H activation, selective poisoning tests were conducted by adding benzyl mercaptan (BzM). BzM binds strongly with Pd, thus preventing Pd-reactant interaction (Fig. 3a and S15).[40] As expected, after introducing 2 equivalents (relative to Pd) BzM to block Pd in Pd/CsPMA before H_2 treatment, PMA was not able to be reduced to enable methane oxidation (BzM-H_2-CH_4/O_2 in Fig. 2e). In contrast, when the same amount of BzM was added to pre-reduced Pd/CsPMA-H catalyst (H_2-BzM-CH_4/O_2 in Fig. 2e), the methanol productivity mimics the performance without BzM. This experiment, together with the earlier presented fact that reduced Rh/CsPMA and Pt/CsPMA are also active in methane oxidation to methanol at room temperature, provide compelling evidence that methane activation proceeds not on Pd sites but on reduced PMA.

The reduced catalyst Pd/CsPMA-H has considerable solubility in H_2O, likely due to the strong interaction between spilt H-induced surface OH groups and water molecules.[51,52] This provides an opportunity to determine whether methanol formation requires an extended surface, or individual PMA anions. Hence, H_2-reduced Pd/CsPMA-H aqueous suspension was separated by ultrafiltration centrifugation (Nominal Molecular Weight Limit: 10 kDa) and evaluated in methane oxidation. The resulting solution and solid residue were both found to offer activity (**Figure S16**), suggesting that H_2-reduced PMA is the active sites for methane conversion, regardless of staying in the solution or solid phase.

To enable catalyst recycling, the spent reaction solution was first re-oxidized by 1 bar O_2 at room temperature, followed by the addition of the Cs^+ salt as a precipitation agent. Over 99% of the Pd/CsPMA catalyst can be regenerated (**Table S6**). A reductive atmosphere (2 bar H_2, 0.3 bar O_2, 10 bar CH_4 diluted with N_2 to a total pressure of 40 bar) was used for reaction sessions during successive recycling tests to ensure sufficient activation of Mo in each cycle. No loss in methanol formation activity was observed over five successive reactions (Fig. 2f), and furthermore the recovered catalyst exhibited identical XRD patterns compared with the fresh one (**Figure S17**), indicating that PMA structure remained intact during recycling.

In view of the important role of reduced PMA on methane activation, we investigated the coordination structure around Mo before and after hydrogen reduction by pseudo *in situ* electron paramagnetic resonance (EPR). As expected, no signal was detected for Pd/CsPMA before H_2 treatment since the Mo species predominantly exist as Mo(VI), which is EPR inactive (**Figure S18**).[49] Measured under the H_2 atmosphere, Pd/CsPMA-H exhibits a broad, featureless EPR spectrum centred at a g value of approximately 1.93 (Fig. 3a), which can be ascribed to the emergence of Mo(V) species.[50–52] The unresolved hyperfine splitting and the asymmetric line shape which almost resemble a broad isotropic line, would point to a Mo(V) centre with six O atoms at close bond lengths where free movement or rotation is relatively unhindered.[53] Afterwards, the EPR tube containing Pd/CsPMA-H was vacuumized and sealed (denoted as Pd/CsPMA-H-vac). The treatment resulted in an anisotropic EPR spectrum with

much narrower line shape and resolution of the splitting arising from the hyperfine interaction of the unpaired electron in Mo(V) with the ^{95}Mo and ^{97}Mo nuclei, both with I = 5/2 and overall natural abundance of 25.5%. This spectral change would imply a large extent of anisotropic distortion of MoO_x polyhedra *in vacuo* (Fig. 3a). Based on simulation results (Fig. 3b, **Figure S19, Table S7**), the spectrum consists of the signals of three Mo(V) components, with the dominant one containing an O vacancy on the bridge site of two MoO_x polyhedra, signified as F (g_1 = 1.955, g_2 = 1.954, g_3 = 1.857, weight = 62%) (**Figure S20**).[54,55] The remaining signals originate from pentacoordinated Mo(V) without molybdenyl oxygen (structure C) and hexacoordinated Mo(V) center (structure A), respectively. Although the results cannot give information on EPR-silent, deep reduced Mo(IV) species, the insights about Mo(V) already provide knowledge on the largely weakened Mo − O bonds and the tendency of O deficiency around Mo centers under reduced state that may facilitate interaction with oxygen or methane molecules.

When Pd/CsPMA-H was exposed to CH_4 and then analyzed by EPR (Fig. 3a), the spectrum exhibited a similar pattern as Pd/CsPMA-H-vac, which illustrates the reduced Mo does not directly coordinate with methane molecules. However, when Pd/CsPMA-H was exposed to air, the EPR signals disappeared immediately. Fully consistent with EPR data, *in situ* Raman experiments reveal that Mo-O_b-Mo and Mo-O_c-Mo are significantly weakened by H_2 reduction, which is recovered after treating with O_2 (**Figure S21**). Based on these, we posit that the MoO_x sites with O vacancies first activate O_2, creating surface active O to then enable C − H activation by abstracting H from methane.

Theoretical insights into the formation of methanol over Pd/CsPMA-H. DFT calculations were performed to further verify potential mechanisms for CH_4 activation and CH_3OH formation over the Pd/CsPMA-H catalyst (Fig. 4 **and Figure S22**). For the creation of active sites, calculations show H_2 activation occurs heterolytically over the Pd single atom site with a relatively low barrier of 0.40 eV, resulting in a OH and PdH species (intermediate **III**). Subsequently, spillover of H to two neighboring oxygen sites is thermodynamically favorable (intermediate **VI**), followed by H_2O generation with a slightly higher barrier of 0.50 eV (intermediate **V**). Upon formation, the H_2O species remains adsorbed bridging two Mo sites, and subsequently desorb to the gas phase which is energetically uphill by 0.81 eV (intermediate **VI**). This results in a lattice oxygen vacancy in the bridging O site which is unreactive towards methane but can readily adsorb O_2 from the gas phase with an adsorption energy of -0.14 eV (intermediate **VII**). In this adsorbed state, one oxygen from O_2 is situated in the lattice O position, while the second oxygen extends away from the surface and does not chemically bond with the surface. The O-O bond length of the adsorbed species is also significantly elongated from the DFT gas-phase length of 1.23 Å to 1.32 Å, suggesting the O_2 has become highly activated and could be reactive to methane. In accordance with this expectation, the C − H activation on the adsorbed O_2 occurs with a barrier of 0.61 eV to form a O_2H species and a CH_3 radical (intermediate **VIII**). Subsequently, the methane radical can be captured by the same O_2H species via a rebound adsorption mechanism to form methanol, simultaneously cleaving the O − O bond and regenerating the lattice oxygen site (intermediate **IX**).

In this mechanism, methane activation is enabled by the formation of activated O_2 species resulting from H spillover and vacancy formation. The rate-limiting step is the C – H activation, in agreement with experimentally observed first-order kinetics for methane. We also find this mechanism to agree with the volcano-type curve for H_2 to O_2 ratio, as a balance must be struck to ensure the survival of the activated O_2 species (intermediate **VI**). An overabundance of gaseous O_2 will react with hydroxyl groups and prevent vacancy formation, while an overabundance of H_2 will likely react with the adsorbed O_2 before it can activate the methane. The mechanism was calculated on oxygen/vacancy sites which are non-adjacent to the Pd, indicating that the presence of Pd was not required for methanol formation beyond the initial H_2 activation step, in accordance with the poisoning studies. Alternative mechanisms were also considered which were found to be unfavorable or inconsistent with experimental observations (**Figure S23-25**, as well as discussions provided there).

Conclusion

In summary, we report a Pd-immobilized PMA catalyst for aerobic methane oxidation to methanol that operates at ambient temperature. Under optimum conditions the catalyst achieved a 29.3 $mmol g_{Pd}^{-1} h^{-1}$ or 67.4 $\mu mol g_{cat}^{-1} h^{-1}$ methanol productivity with nearly 100% selectivity at room temperature. The active sites are partially reduced Mo on PMA bearing O vacancies at the bridge sites, which readily activates O_2 by a refilling mechanism, creating active O for H abstraction from methane. Pd enables H_2 activation and PMA reduction, but does not participate in methane conversion. The finding provides a system for the selective methanol synthesis from methane using molecular O_2 as the oxidant at ambient temperature without the use of an external energy source (*e.g.*, light, electricity). From a mechanism perspective, the Mo centre under partially reduced state is found to be critical for an oxidation reaction to generate active oxygen species from O_2, which extends our understanding of typical catalytic oxidation processes.

Declarations

CRediT authorship contribution statement

N.Y. conceived and supervised the project. Q.H. and G.J.H co-supervised the project. S.W. conducted most experiments including synthesis, characterization, and testing, as well as data analysis. V.F carried out DFT calculations and wrote the related section. M.J.H. and J.C. participated catalyst synthesis and characterizations. X.L. and Z.Y. conducted TEM analysis. A.F. and R.J.L. contributed to data analysis of EPR spectra and H_2O_2 detection. S.W., Q.H. and N.Y. wrote the manuscript. G.J.H, A.F. and R.J.L. revised the manuscript. All authors discussed the manuscript.

Declaration of Competing Interest

The authors declare that they have no known competing financial interests or personal relationships that could have appeared to influence the work reported in this paper.

Acknowledgement

We thank National Natural Science Foundation of China (92061109) for supporting the project. N.Y and Q.H sincerely acknowledge the support of the National Research Foundation (NRF) Singapore, under its NRF Investigatorship (NRF-NRFI07–2021–0006) and NRF Fellowship (NRF-NRFF11-2019-0002), respectively. R.J.L and G.J.H gratefully acknowledge Cardiff University and the Max Planck Centre for Fundamental Heterogeneous Catalysis (FUNCAT) for financial support. Z.Y. acknowledge support from the National Natural Science Foundation of China (52222102, 22272024 and 51871058) and the Eyas Program of Fujian Province. DFT simulations were conducted at the Center for Nanophase Materials Sciences (CNMS), which is a US Department of Energy, Office of Science User Facility at Oak Ridge National Laboratory.

References

1. Sushkevich, V. L., Palagin, D., Ranocchiari, M. & Bokhoven, J. A. v. Selective anaerobic oxidation of methane enables direct synthesis of methanol. *Science* **356**, 523-527, (2017).
2. Shan, J., Li, M., Allard, L. F., Lee, S. & Flytzani-Stephanopoulos, M. Mild oxidation of methane to methanol or acetic acid on supported isolated rhodium catalysts. *Nature* **551**, 605-608, (2017).
3. Schwach, P., Pan, X. & Bao, X. Direct Conversion of Methane to Value-Added Chemicals over Heterogeneous Catalysts: Challenges and Prospects. *Chem. Rev.* **117**, 8497-8520, (2017).
4. Wang, V. C. *et al.* Alkane Oxidation: Methane Monooxygenases, Related Enzymes, and Their Biomimetics. *Chem. Rev.* **117**, 8574-8621, (2017).
5. Meng, X. *et al.* Direct Methane Conversion under Mild Condition by Thermo-, Electro-, or Photocatalysis. *Chem* **5**, 2296-2325, (2019).
6. Sher Shah, M. S. A. *et al.* Catalytic Oxidation of Methane to Oxygenated Products: Recent Advancements and Prospects for Electrocatalytic and Photocatalytic Conversion at Low Temperatures. *Advanced Science* **7**, 2001946, (2020).
7. IEA, Resources to Reserves 2013, Paris, (2013).
8. Koo, C. W. & Rosenzweig, A. C. Biochemistry of aerobic biological methane oxidation. *Chem. Soc. Rev.* **50**, 3424-3436, (2021).
9. Hammond, C. *et al.* Direct catalytic conversion of methane to methanol in an aqueous medium by using copper-promoted Fe-ZSM-5. *Angew. Chem. Int. Ed.* **51**, 5129-5133, (2012).
10. Qi, G. *et al.* Au-ZSM-5 catalyses the selective oxidation of CH4 to CH3OH and CH3COOH using O2. *Nat. Catal.* **5**, 45-54, (2022).
11. Baek, J. *et al.* Bioinspired Metal-Organic Framework Catalysts for Selective Methane Oxidation to Methanol. *J. Am. Chem. Soc.* **140**, 18208-18216, (2018).
12. Ikuno, T. *et al.* Methane Oxidation to Methanol Catalyzed by Cu-Oxo Clusters Stabilized in NU-1000 Metal-Organic Framework. *J. Am. Chem. Soc.* **139**, 10294-10301, (2017).

13. Zheng, J. *et al.* Selective Methane Oxidation to Methanol on Cu-Oxo Dimers Stabilized by Zirconia Nodes of an NU-1000 Metal-Organic Framework. *J. Am. Chem. Soc.* **141**, 9292-9304, (2019).
14. Osadchii, D. Y. *et al.* Isolated Fe Sites in Metal Organic Frameworks Catalyze the Direct Conversion of Methane to Methanol. *ACS Catal.* **8**, 5542-5548, (2018).
15. Huang, W. *et al.* Low-Temperature Transformation of Methane to Methanol on Pd1O4 Single Sites Anchored on the Internal Surface of Microporous Silicate. *Angew. Chem. Int. Ed.* **55**, 13441-13445, (2016).
16. Kwon, Y., Kim, T. Y., Kwon, G., Yi, J. & Lee, H. Selective Activation of Methane on Single-Atom Catalyst of Rhodium Dispersed on Zirconia for Direct Conversion. *J. Am. Chem. Soc.* **139**, 17694-17699, (2017).
17. Cui, X. *et al.* Room-Temperature Methane Conversion by Graphene-Confined Single Iron Atoms. *Chem* **4**, 1902-1910, (2018).
18. Shen, Q. *et al.* Single Chromium Atoms Supported on Titanium Dioxide Nanoparticles for Synergic Catalytic Methane Conversion under Mild Conditions. *Angew. Chem. Int. Ed.* **59**, 1216-1219, (2020).
19. Bai, S. *et al.* High-efficiency direct methane conversion to oxygenates on a cerium dioxide nanowires supported rhodium single-atom catalyst. *Nat. Commun.* **11**, 954, (2020).
20. Tang, X. *et al.* Direct oxidation of methane to oxygenates on supported single Cu atom catalyst. *Appl. Catal. B: Environ.* **285**, 119827, (2021).
21. Ab Rahim, M. H. *et al.* Oxidation of methane to methanol with hydrogen peroxide using supported gold-palladium alloy nanoparticles. *Angew. Chem. Int. Ed.* **52**, 1280-1284, (2013).
22. Agarwal, N. *et al.* Aqueous Au-Pd colloids catalyze selective CH₄ oxidation to CH₃OH with O₂ under mild conditions. *Science* **358**, 223-227, (2017).
23. Chen, J. *et al.* Oxidation of methane to methanol over Pd@Pt nanoparticles under mild conditions in water. *Catal. Sci. Technol.* **11**, 3493-3500, (2021).
24. He, Y. *et al.* Low-temperature direct conversion of methane to methanol over carbon materials supported Pd-Au nanoparticles. *Catal. Today* **339**, 48-53, (2020).
25. Bai, S., Xu, Y., Wang, P., Shao, Q. & Huang, X. Activating and Converting CH4 to CH3OH via the CuPdO2/CuO Nanointerface. *ACS Catal.* **9**, 6938-6944, (2019).
26. Wu, B. *et al.* Cu single-atoms embedded in porous carbon nitride for selective oxidation of methane to oxygenates. *Chem. Commun.* **56**, 14677-14680, (2020).
27. Xie, J. *et al.* Highly selective oxidation of methane to methanol at ambient conditions by titanium dioxide-supported iron species. *Nat. Catal.* **1**, 889-896, (2018).
28. McVicker, R. *et al.* Low temperature selective oxidation of methane using gold-palladium colloids. *Catal. Today* **342**, 32-38, (2020).
29. Jin, Z. *et al.* Hydrophobic zeolite modification for in situ peroxide formation in methane oxidation to methanol. *Science* **367**, 193, (2020).

30. Kang, J. & Park, E. D. Selective Oxidation of Methane over Fe-Zeolites by In Situ Generated H2O2. *Catalysts* **10**, 299, (2020).
31. Kang, J., Puthiaraj, P., Ahn, W.-s. & Park, E. D. Direct synthesis of oxygenates via partial oxidation of methane in the presence of O2 and H2 over a combination of Fe-ZSM-5 and Pd supported on an acid-functionalized porous polymer. *Appl. Catal. A: Gen.* **602**, 117711, (2020).
32. Luo, L. *et al.* Synergy of Pd atoms and oxygen vacancies on In(2)O(3) for methane conversion under visible light. *Nat. Commun.* **13**, 2930, (2022).
33. An, B. *et al.* Direct photo-oxidation of methane to methanol over a mono-iron hydroxyl site. *Nat. Mater.* **21**, 932-938, (2022).
34. Fan, Y. *et al.* Selective photocatalytic oxidation of methane by quantum-sized bismuth vanadate. *Nat. Sustain.* **4**, 509-515, (2021).
35. Srivastava, R. K., Sarangi, P. K., Bhatia, L., Singh, A. K. & Shadangi, K. P. Conversion of methane to methanol: technologies and future challenges. *Biomass Convers. Biorefin.* **12**, 1851-1875, (2021).
36. Lopez, X., Carbo, J. J., Bo, C. & Poblet, J. M. Structure, properties and reactivity of polyoxometalates: a theoretical perspective. *Chem. Soc. Rev.* **41**, 7537-7571, (2012).
37. Wang, S.-S. & Yang, G.-Y. Recent Advances in Polyoxometalate-Catalyzed Reactions. *Chem. Rev.* **115**, 4893-4962, (2015).
38. Zhang, B. *et al.* Stabilizing a Platinum1 Single-Atom Catalyst on Supported Phosphomolybdic Acid without Compromising Hydrogenation Activity. *Angew. Chem. Int. Ed.* **55**, 8319-8323, (2016).
39. Zhang, B. *et al.* Atomically Dispersed Pt1-Polyoxometalate Catalysts: How Does Metal-Support Interaction Affect Stability and Hydrogenation Activity? *J. Am. Chem. Soc.* **141**, 8185-8197, (2019).
40. Hülsey, M. J., Fung, V., Hou, X., Wu, J. & Yan, N. Hydrogen spillover and its relation to hydrogenation: observations on structurally defined single-atom sites. *Angew. Chem. Int. Ed.* **n/a**.
41. Hülsey, M. J. *et al.* Identifying Key Descriptors for the Single-atom Catalyzed CO Oxidation. *CCS Chem.* **4**, 1-24.
42. Geng, Y. & Li, H. Hydrogen Spillover-Enhanced Heterogeneously Catalyzed Hydrodeoxygenation for Biomass Upgrading. *ChemSusChem*, e202102495, (2022).
43. Xiong, M., Gao, Z. & Qin, Y. Spillover in Heterogeneous Catalysis: New Insights and Opportunities. *ACS Catal.* **11**, 3159-3172, (2021).
44. Xi, Q. *et al.* In-situ fabrication of MoO3 nanobelts decorated with MoO2 nanoparticles and their enhanced photocatalytic performance. *Appl. Surf. Sci.* **480**, 427-437, (2019).
45. Dieterle, M., Weinberg, G. & Mestl, G. Raman spectroscopy of molybdenum oxides. *Phys. Chem. Chem. Phys.* **4**, 812-821, (2002).
46. Ravi, M. *et al.* Misconceptions and challenges in methane-to-methanol over transition-metal-exchanged zeolites. *Nat. Catal.* **2**, 485-494, (2019).
47. Richards, T. *et al.* A residue-free approach to water disinfection using catalytic in situ generation of reactive oxygen species. *Nat. Catal.* **4**, 575-585, (2021).

48. Fontmorin, J. M., Burgos Castillo, R. C., Tang, W. Z. & Sillanpaa, M. Stability of 5,5-dimethyl-1-pyrroline-N-oxide as a spin-trap for quantification of hydroxyl radicals in processes based on Fenton reaction. *Water Res.* **99**, 24-32, (2016).
49. Cozar, O., Magdas, D. A. & Ardelean, I. EPR study of molybdenum-lead-phosphate glasses. *J. Non. Cryst. Solids* **354**, 1032-1035, (2008).
50. Triwahyono, S., Jalil, A. A., Ruslan, N. N., Setiabudi, H. D. & Kamarudin, N. H. N. C5–C7 linear alkane hydroisomerization over MoO3–ZrO2 and Pt/MoO3–ZrO2 catalysts. *J. Catal.* **303**, 50-59, (2013).
51. Almidani, A. H. *et al.* The reaction of HV(CO)4dppe with MoO3: a well-defined model of hydrogen spillover. *Catal. Sci. Technol.* **11**, 7540-7544, (2021).
52. Timmiati, S. N., Jalil, A. A., Triwahyono, S., Setiabudi, H. D. & Annuar, N. H. R. Formation of acidic Brönsted (MoOx)−(Hy)+ evidenced by XRD and 2,6-lutidine FTIR spectroscopy for cumene cracking. *Appl. Catal. A: Gen.* **459**, 8-16, (2013).
53. Spencer, J., Folli, A., Richards, E. & Murphy, D. M. *Applications of electron paramagnetic resonance spectroscopy for interrogating catalytic systems*. Vol. 26 (2018).
54. Labanowska, M. EPR Monitoring of Redox Processes in Transition Metal Oxide Catalysts. *ChemPhysChem* **2**, 712-731, (2001).
55. Łabanowska, M. Paramagnetic defects in MoO3—revisited. *Phys. Chem. Chem. Phys.* **1**, 5385-5392, (1999).

Figures

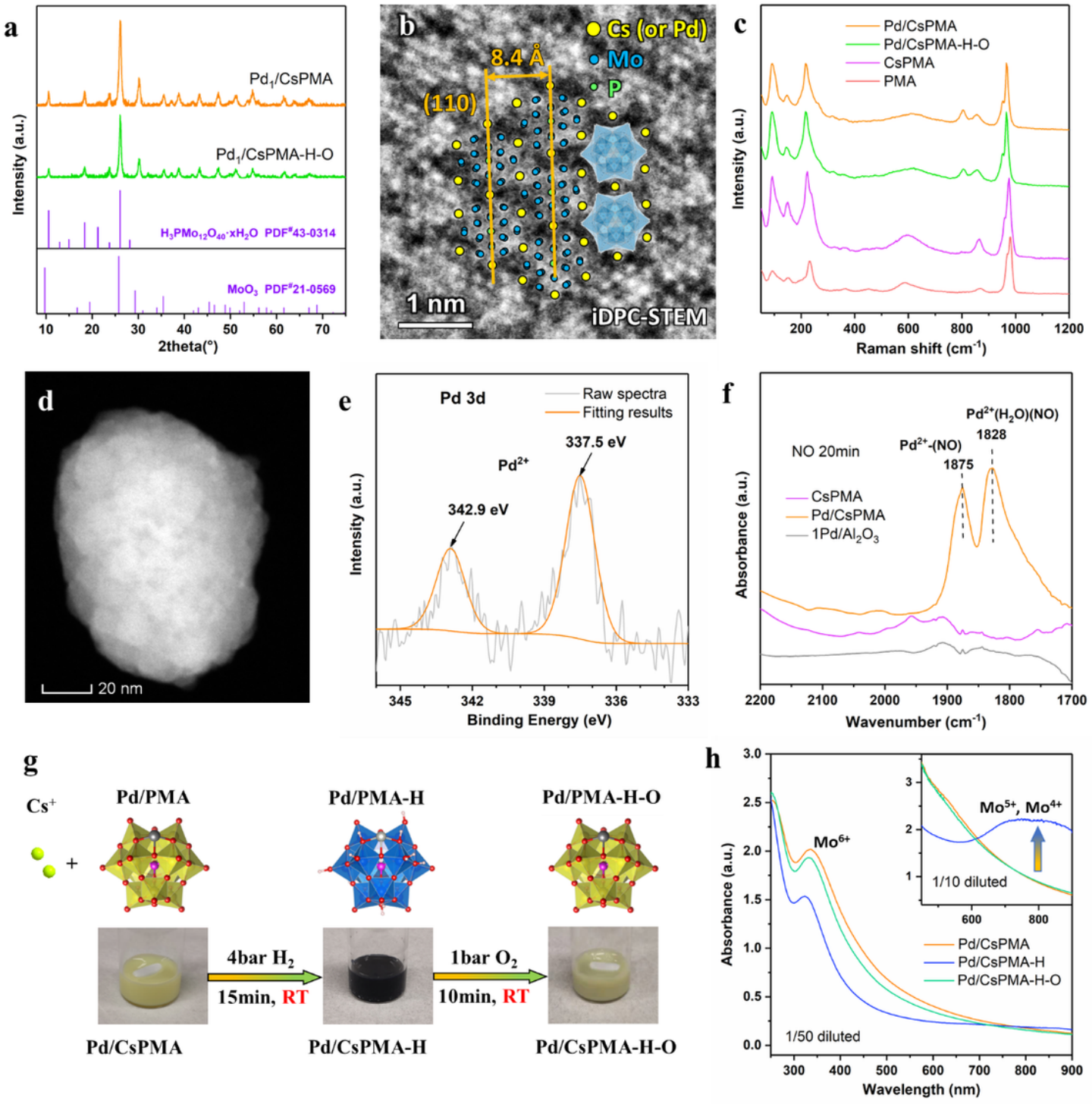

Figure 1

Structure and redox properties of Pd/CsPMA. (a) XRD spectra of Pd/CsPMA, Pd/CsPMA-H-O, and the standard XRD lines of $H_3PMo_{12}O_{40}$ (PMA) and MoO_3. (b) High resolution TEM image of Pd/CsPMA. The insert shows the electron diffraction pattern in the area. (c) Raman spectra of PMA, CsPMA, Pd/CsPMA and Pd/CsPMA-H-O. (d) HAADF-STEM image of Pd/CsPMA. (e) Experimental and fitting results of Pd 3d XPS spectra of Pd/CsPMA. (f) *In situ* NO-DRIFTS spectra of CsPMA, Pd/CsPMA and the commercial 1

wt% Pd/Al_2O_3. (g) The reversible reduction/oxidation of Pd/CsPMA at room temperature. (h) UV-Vis adsorption spectra of the suspensions of Pd/CsPMA and Pd/CsPMA-H.

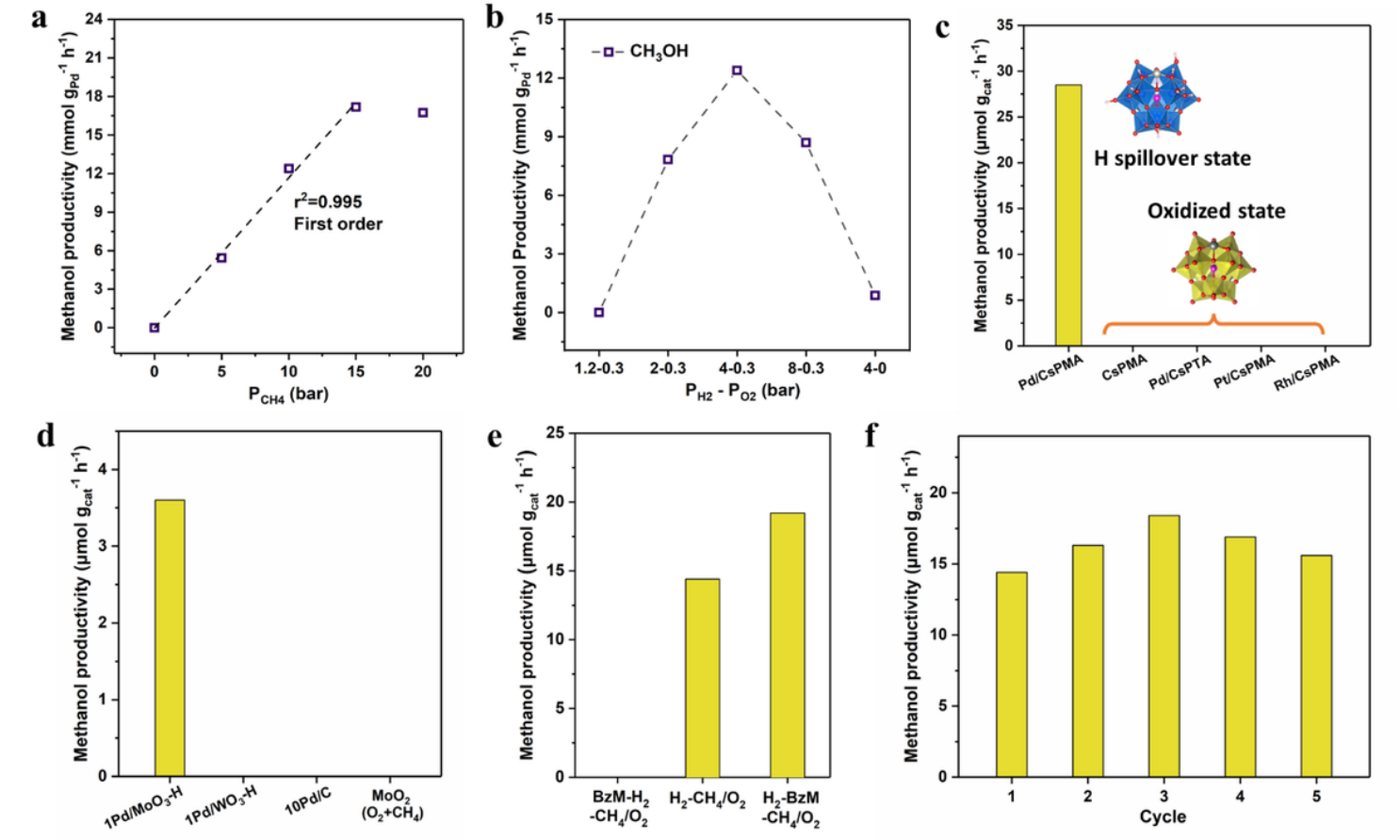

Figure 2

Parameter-activity correlations and recycling tests of methane oxidation to methanol in a CH_4, H_2, and O_2 mixture. Reaction condition: 10 mg catalyst in 2 ml D_2O, 4 bar H_2, 0.3 bar O_2, 10 bar CH_4 balanced with 25.7 bar N_2, room temperature, 30 min, unless otherwise specified. (a) Methanol productivity under varied CH_4 partial pressure using Pd/CsPMA. (b) Methanol productivity under varied partial pressures of H_2 and O_2. (c) Methanol productivity for different POM-based catalysts. The loading of noble metals on the supported catalysts are around 0.25 wt%. (d) Methanol productivity using several traditional catalysts. For 1Pd/MoO_3-H and 1Pd/WO_3-H, the impregnated samples are treated with 5%H_2/N_2 at 300 °C. For MoO_2, 1 bar O_2, 10 bar CH_4 and 9 bar N_2 were supplied without addition of H_2. (e) Poisoning tests using benzyl mercaptan (BzM) to block Pd sites (reaction condition is the same as annotated in Table 1, Entry 3). BzM dissolved in ethanol was added into the reaction mixture before or after H_2 treatment (BzM:Pd = 2:1). For the control experiment without BzM, same amount of ethanol solvent was added after H_2 pretreatment before methane conversion. (f) Recyclability test of Pd/CsPMA for methane oxidation with O_2 and H_2 (2 bar H_2, 0.3 bar O_2, 10 bar CH_4, 30 mins).

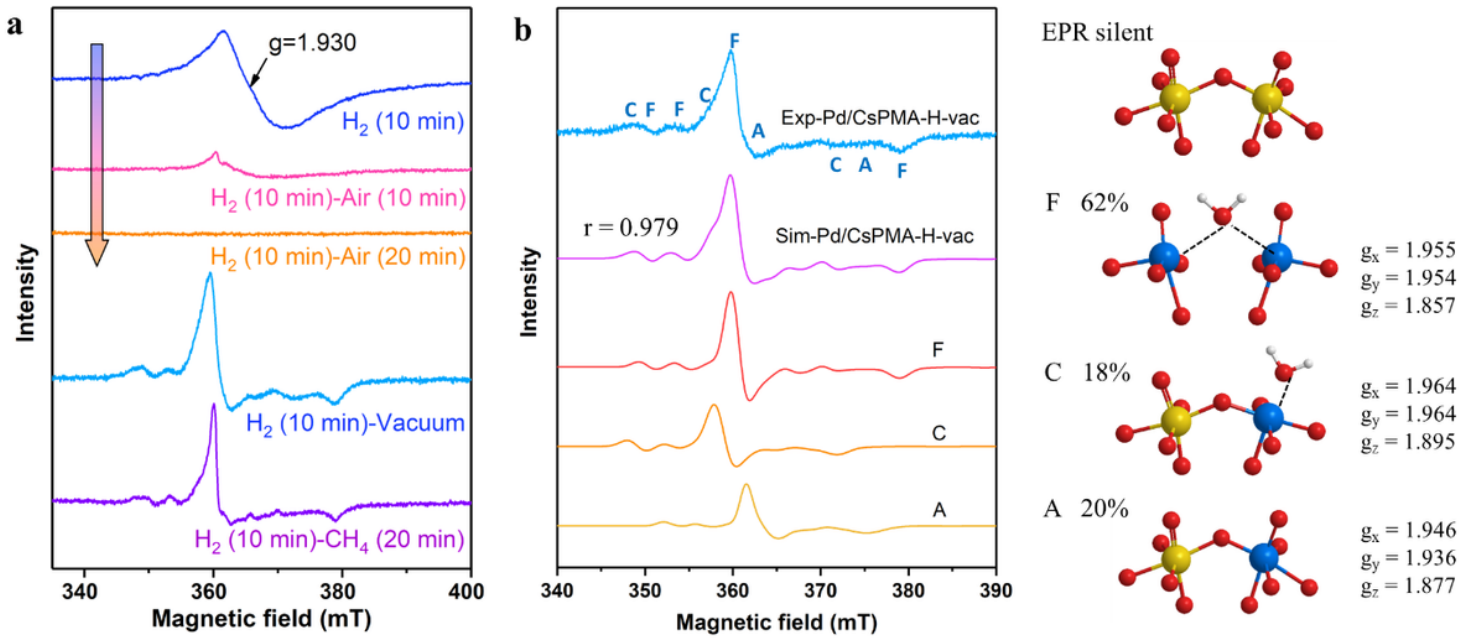

Figure 3

Dynamic structural changes of Mo species in varied atmosphere revealed by EPR. (a) Pseudo *in situ* EPR spectra of Pd/CsPMA catalyst after treating by different gases for different times. “Air” refers to removing the cover of the EPR tube and allowing the air to diffuse towards the catalyst at the bottom of the EPR tube. (b) Experimental and simulated EPR spectra of Pd/CsPMA-H solid under vacuo. The deconvoluted spectra are presented with corresponding g value, weight and local structure listed on the right. Red, yellow and blue balls represent H, Mo(VI) and Mo(V) respectively.

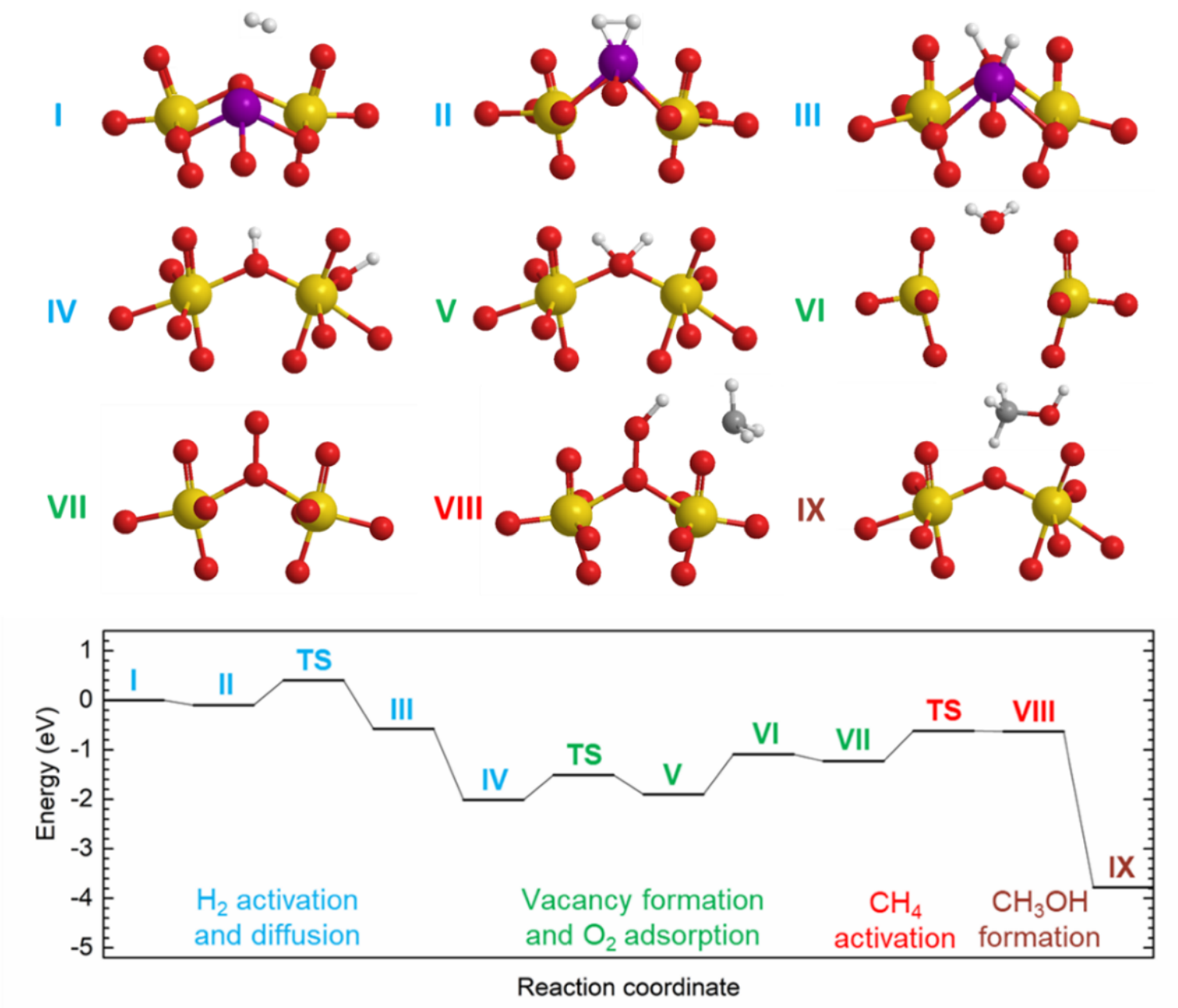

Figure 4

Proposed reaction mechanism for CH_4 activation and CH_3OH formation from DFT calculations. The reaction first proceeds via H_2 activation and diffusion (intermediates **I**, **II**, and **III**), followed by vacancy formation and O_2 adsorption (intermediates **IV**, **V**, **VI**), then CH_4 activation (intermediate **VII**) and CH_3OH formation (intermediates **VIII** and **IX**).

Supplementary Files

This is a list of supplementary files associated with this preprint. Click to download.

- SI.pdf